Materials and Design 161 (2019) 44–54

Contents lists available at ScienceDirect

Materials and Design

journal homepage: www.elsevier.com/locate/matdes

Surface functionalization of 3D printed polymer scaffolds to augment stem cell response

L.R. Jaidev, Kaushik Chatterjee *

Department of Materials Engineering, Indian Institute of Science, Bangalore 560012, India

HIGHLIGHTS

- 3D printed scaffolds of poly(lactic acid) with 70% porosity were prepared by materials extrusion.
- Scaffold surface was modified by grafting polyethyleneimine and citric acid followed by deposition of calcium phosphate.
- Scaffolds released calcium ions and exhibited enhanced roughness and water wettability after surface modification.
- Adhesion and proliferation of mesenchymal stem cells increased by 50% after surface modification.
- Enhanced stem cell osteogenesis on the surface modified scaffolds resulted in doubling of the mineralization.

GRAPHICAL ABSTRACT

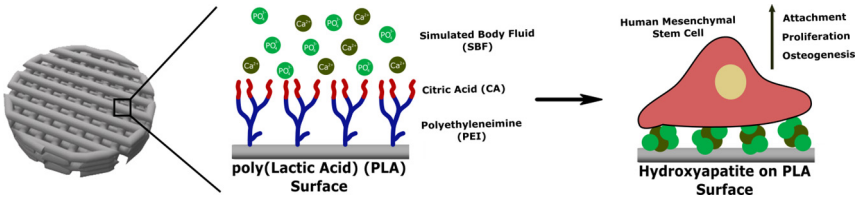

ARTICLE INFO

Article history:
Received 14 August 2018
Received in revised form 6 November 2018
Accepted 7 November 2018
Available online 8 November 2018

Keywords:
3D printing
Tissue scaffold
Surface engineering
Hydroxyapatite
Stem cells

ABSTRACT

Three-dimensional (3D) printing by material extrusion is being widely explored to prepare patient-specific scaffolds from biodegradable polyesters such as poly(lactic acid) (PLA). Although they provide the desired mechanical support, PLA scaffolds lack bioactivity to promote bone regeneration. The aim of this work was to develop a surface engineering approach for enhancing the osteogenic activity of 3D printed PLA scaffolds. Macro-porous PLA scaffolds were prepared by material extrusion with 70.2% porosity. Polyethyleneimine was chemically conjugated to the alkali-treated PLA scaffolds followed by conjugation of citric acid. These polymer-grafted scaffolds were immersed in the simulated body fluid to yield scaffolds coated with calcium-deficient hydroxyapatite (PLA-HaP). Surface roughness and water wettability were enhanced after surface modification. PLA-HaP scaffolds exhibited a steady release of calcium ions in an aqueous medium for 10 days. The adhesion and proliferation of human mesenchymal stem cells (hMSCs) on PLA-HaP was ~50% higher than on PLA. Mineral deposition resulting from hMSC osteogenesis on PLA-HaP scaffolds was nearly twice that on PLA scaffolds. This was corroborated by the increase in alkaline phosphatase activity and expression of several osteogenic genes. Thus, this work presents a surface modification strategy to enhance the bioactivity of 3D printed scaffolds for bone tissue regeneration.

1. Introduction

Bone is one of the most widely transplanted tissues around the world [1]. The recent advent of three-dimensional (3D) printing offers hitherto unavailable opportunities to develop the next-generation

* Corresponding author.
E-mail address: kchatterjee@iisc.ac.in (K. Chatterjee).

https://doi.org/10.1016/j.matdes.2018.11.018

bone tissue grafts with significant advantages over conventional grafts [2]. Personalized implants can be fabricated with dimensions tailored to suit the anatomy of individual patients [3]. Near-net shapes can also be achieved to closely match the defect dimensions [4]. 3D printing can be employed for the development of porous polymeric scaffolds to augment bone repair and tissue regeneration as alternatives to tissue grafts [5].

An ideal bone scaffold should mimic the extracellular matrix (ECM) of bone consisting of collagen and calcium phosphate (CaP) deposits in the form of hydroxyapatite (HaP) to provide cues for augmenting the response of stem/progenitor cells such as attachment, proliferation and differentiation for bone formation and eventual osseointegration at the implanted site [6,7]. Additively manufactured polymeric scaffolds offer an unprecedented combination of mechanical strength, controlled architecture and tailored porosity [8]. Owing to its ease of use and affordability, material extrusion (or fused filament fabrication) is one of the most popular 3D printing techniques [9]. Material extrusion is widely used for 3D printing of polyesters where the polymer filament is melted at high temperature and deposited in a layer-by-layer manner to achieve a 3D architecture without the need for a binder solution [10]. Several researchers have reported the preparation of porous scaffolds prepared by material extrusion and demonstrated their advantages for bone tissue engineering [11–13]. Materials extrusion was used to 3D printed scaffolds of poly(lactic acid) (PLA) with graded microstructures for bone tissue regeneration [11]. 3D printed scaffolds with nanoparticle fillers for bone regeneration have also been proposed [13]. Polyesters such as PLA [14], polycaprolactone (PCL) [15] and polylactide-*co*-glycolide (PLGA) [16], etc., constitute a popular class of biodegradable polymers for 3D printing of scaffolds. The facile use of polyesters for 3D printing has equipped researchers to develop 3D printed scaffolds incorporated with unique nanomaterials such as calcium phosphate [20], calcium silicate [21], mesoporous silica [22], and bioglass [23,24], etc. However, processing of the feed material typically in the form of a powder or a filament using heat or harsh chemicals to prepare the scaffold by 3D printing essentially precludes the incorporation of labile biomolecules such as growth factors and several drugs to stimulate the cells.

There is a need to engineer surface modification techniques to augment the poor bioactivity of the 3D printed scaffolds, which otherwise offer several benefits. To address this challenge a few strategies have been proposed such as surface roughening for increased cell proliferation [9], peptide modification of the scaffold surface [10], surface modification using hyaluronic acid and collagen [17], and the use of mussel adhesive proteins for better cell attachment [16], etc. We and others have shown previously, that the controlled release of bioactive ions such as calcium [18], strontium [19], silicon [20], silver [21] and copper [22] ions from nanoparticles in the polymeric scaffolds can impart bioactivity such as enhanced osteogenic, angiogenic and antimicrobial properties, etc. One strategy to improve the bioactivity of printed scaffolds has been the incorporation of CaP as a filler in polymer composites [23]. Similar strategies were adapted by several groups for functionalization of 3D printed scaffolds [13,24,25]. However, a large fraction of CaP is trapped within the slowly degrading polymer matrix and is not readily available to the cells at the cell-material interface. As an alternate strategy, we aimed to form CaP coating on the scaffold surface by incubation in simulated body fluid (SBF) [26].

Neat PLA surface is not ideal for inducing the formation of hydroxyapatite but it can be modified by surface grafting of functional moieties to facilitate mineralization on the surface. Citric acid (CA) is a minor component of bones and plays a critical role in precipitating the apatite phase during bone formation [27]. Sun et al. demonstrated the utility of composite scaffolds prepared from CA and HaP for the regeneration of the calvarial bone defects [28]. Deposition of HaP minerals on the surface of the scaffolds can be achieved by CA-mediated precipitation of calcium and phosphate ions from SBF [29]. It was shown that HaP was formed on the collagen membrane by CA-assisted precipitation when immersed in SBF. Polyethyleneimine (PEI) is an amine-rich polymer widely used in various biomedical applications and has been employed in bone tissue engineering because of its ability to facilitate cell proliferation and osteogenesis [30]. The amine functional groups of PEI can facilitate conjugation of biomolecules [31] or even CA to the polyester.

Toward developing a versatile and potent strategy for the surface modification of 3D printed scaffolds for augmenting bone regeneration, the present study aimed to prepare porous PLA scaffolds surface modified with HaP. PLA scaffolds were 3D printed by material extrusion. Subsequently, PEI was conjugated to the surface of the scaffold and it was further used for grafting CA. Apatite minerals were deposited by immersing in SBF. The physico-chemical properties of the surface modified scaffolds were characterized and the osteogenic abilities were evaluated using hMSCs.

2. Materials and methods

2.1. Materials

PLA filament of 1.75 mm diameter was purchased from Reddx Technologies, India. PEI (branched low mol. wt. M_n ~1800) was procured from Sigma Aldrich. CA, *N*-hydroxysuccinimide (NHS) and 1-ethyl-3-(3-dimethylaminopropyl) carbodiimide (EDC) were purchased from Merck. All chemicals were of analytical grade and used without further modifications.

2.2. Fabrication of PLA scaffolds by 3D printing

A 3D printer (FabX3.0, Reddx Technologies, India) was used to fabricate 3D porous scaffolds. These material extrusion-based 3D printers melt a polymer filament to lay the polymer in layer-by-layer fashion without any necessity of using binder for fabricating the scaffold with controlled arrangement of the struts and pore dimensions in the scaffold. The machine has an integrated feeder system that feeds the PLA filament. The dispensing system is the extrusion nozzle (E3Dlite extruder, 0.4 mm diameter) controlled by stepper motors in x- and y-directions while the base collection plate moves in the z-direction. The computer aided design (CAD, Sketchup make) approach was used to design circular 3D scaffolds. The circular scaffolds were designed in orthogonal layer configuration with dimensions 8.9 mm × 2.0 mm (diameter × height), the distance between the struts axes (d1) of 500 μm and the diameter or road width (Rw) of the struts 500 μm with the final pore area of 0.25 mm^2. The orthogonal scaffold architecture was designed in a lay-down pattern of 0°/90° forming square pores. The 3D scaffolds were prepared by plotting layer-by-layer by the melt extrusion of the PLA filament from the extruder nozzle at the speed of 40 $mm \cdot s^{-1}$. The temperature at the extrusion nozzle was maintained at 220 °C.

2.3. Surface functionalization of 3D printed PLA scaffolds

The 3D printed PLA scaffolds were immersed in 5.0 M NaOH for 1 h, as reported earlier [32]. The scaffolds were washed repeatedly with ultrapure water until the pH was 7.0. Note that the 3D printed porous scaffolds are hereafter referred to as PLA scaffolds whereas scaffolds after NaOH treatment are denoted as PLA-OH. The scaffolds were air dried and stored in a dry place before each subsequent surface modification step respectively.

Low molecular weight branched PEI was conjugated to the PLA-OH scaffolds using carbodiimide (EDC-NHS) chemistry. 1 g of PLA-OH scaffolds in 100 mL of deionized water containing 1 mM of EDC and NHS were stirred for 1 h at 4 °C. 1 g PEI was added and stirred overnight at 23 °C. The unreacted PEI was removed by washing with water. These scaffolds are hereafter referred to as PLA-PEI.

The PLA-PEI scaffolds were further functionalized by conjugating CA to the amine groups of PEI via EDC-NHS chemistry, as described above. After incubation with EDC and NHS, 3 g CA was added and stirred

overnight at 23 °C. The unreacted CA was removed by washing with water and these scaffolds are hereafter referred to as PLA-CA.

The PLA-CA scaffolds were immersed and incubated in 1.5 SBF with ionic concentration similar to that of human blood plasma [26] for 7 days at 37 °C. These scaffolds are hereafter referred to as PLA-HaP were washed twice with deionized water, air dried and stored in a dry place until further use.

2.4. Characterization of 3D printed scaffolds

A scanning electron microscope (SEM, ESEM Quanta 200, FEI) was used to characterize the surface topography of the 3D printed scaffolds. The scaffold architecture was characterized by X-ray micro-computed tomography (microCT, XRADIA, Zeiss) set at 60 V, 5 A and imaged at a pixel size of 11 μm with a total of 1101 image slices. Porosity was quantified using the Avizo 8 software. The morphological changes on the surface of PLA and PLA-OH were characterized using an atomic force microscope (AFM, NX-10, Park Systems). The confirmation of surface functionalization of PEI and CA on PLA was studied using X-ray photoelectron spectroscopy (XPS, Axis Ultra, Kratos Analytical). The water wettability of the scaffolds was evaluated using sessile drop technique by depositing ultrapure water of 2 μl on the surface of the polymer strut and analyzed after 5 s using a contact angle goniometer (OCA 15 plus, Data physics). The contact angle was measured on three independent samples at 23 °C. The HaP deposits on the PLA-HaP scaffolds were quantified using a thermogravimetric analyzer (TGA, Q 500, TA instruments). The crystalline nature of the deposited hydroxyapatite was characterized by X-ray diffraction (XPERTPro, PANalytical, UK) with Cu Kα radiation source ($\lambda = 1.5406$ Å, 40 kV, and 20 mA) with a 2θ range of 20° to 40°.

2.5. Mechanical properties of 3D printed scaffolds

The compressive modulus was measured using a universal testing machine (Instron 5967) with a 5 kN load cell with a crosshead speed of 1 mm/min without any preloading. The compressive modulus of the scaffolds (dimensions of 8.8 mm diameter and 11.5 mm height) was determined by calculating the slope of the stress-strain curve in the elastic region.

2.6. Calcium release

The release of calcium ions from the PLA-HaP scaffolds was studied for 10 days. The scaffolds were taken in a 48 well plate with 1 mL PBS (pH 7.4) and incubated in a temperature-controlled incubator (Biogenics) set at 37 °C. At every 24 h interval, PBS was collected from each well and replenished with fresh PBS. The ion concentration in the solutions was analyzed using inductively coupled plasma - optical emission spectrometry (ICP-OES, iCAP 7000, Thermo Scientific) and determined by comparison with a standard curve that was generated using solutions of known calcium concentration.

2.7. Stem cell adhesion and proliferation on scaffolds

Primary bone marrow-derived hMSCs were used for this work and their response was studied using a combination of standard assays and imaging techniques as briefly described here. Complete details are presented in Supporting Information. The scaffolds were sterilized and seeded with 2.5×10^4 hMSCs in 48 well plates. Cells were fixed and observed in SEM to assess their morphology. Separately, fixed cells were stained with propidium iodide and Phalloidin Alexa fluor 488 to visualize the nuclei and F-actin under a laser scanning confocal microscope. WST-1 assay was used to assess the proliferation of hMSCs on the scaffolds.

2.8. Osteogenesis studies

Stem cell osteogenesis was studied by assaying the alkaline phosphatase (ALP) activity on day 14. The ALP activity was normalized to the total protein content determined by the microBCA protein assay. Furthermore, we assessed mineral deposition using alizarin red staining. The mineral content was normalized to cell numbers.

2.9. Gene expression of osteogenic markers

The expression of the osteogenic markers such as bone morphogenic protein-2 (BMP-2), runt-related transcription factor 2 (RUNX2), osteocalcin (OCN) and alkaline phosphatase (ALP) genes was studied using real time qRT-PCR with GAPDH as the house-keeping gene. The primers used are tabulated in Table S1.

2.10. Statistics

Two-way ANOVA with Tukey's test was performed to find the difference of significance between the treatments and respective time points. One-way ANOVA with Tukey's test was done to find significant differences ($p < 0.05$) between the samples.

3. Results

3.1. Fabrication of 3D printed PLA scaffolds

Fig. 1A presents the 3D printer used in this work to fabricate the porous PLA scaffolds. The CAD model of the circular scaffold of orthogonal layer configuration with the lay-down pattern of 0/90° following the in-line vertical architecture was used owing to its better mechanical properties [15,24] as shown in Fig. 1B whereas Fig. 1C shows the final 3D printed scaffold. The final dimensions of the 3D printed PLA scaffold was 8.9 ± 0.04 mm in diameter and 1.9 ± 0.04 mm height, which closely match the dimensions in the CAD file. The 0/90° in-line architecture and porosity of the as-printed scaffolds were analyzed with microCT (Fig. 1D & Fig. S1). The porosity was determined to be 70.2% with an open porous architecture.

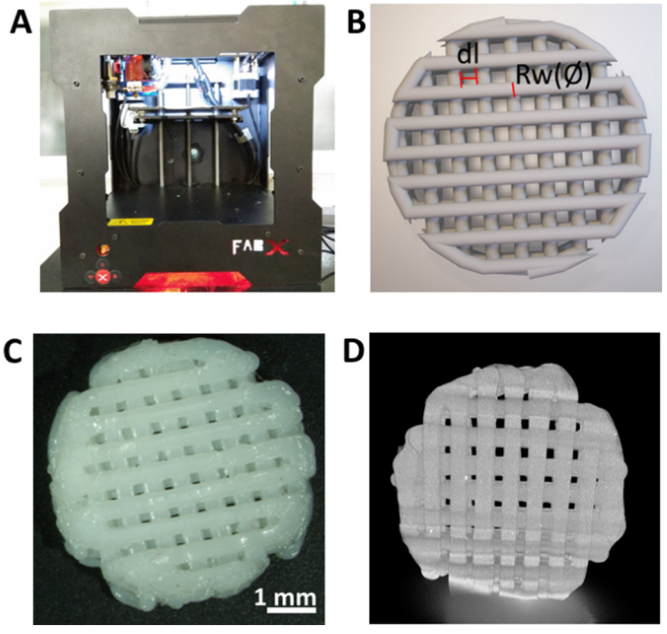

Fig. 1. 3D printing of PLA scaffolds [A] The 3D printer used in this work; [B] Designed CAD model of the scaffold (dl is the distance between the struts and the width of each strut (Rw) is the diameter of the strut); [C] Optical image of the PLA 3D scaffold and [D] MicroCT image of the PLA scaffold showing the porous architecture of the scaffold.

The surface of the PLA 3D scaffolds was hydrophobic and exhibiting a water contact angle of 124 ± 5° in good agreement with the known hydrophobic nature of PLA. The wettability of the 3D printed PLA scaffolds was improved with NaOH treatment and the resultant water contact angle was lowered to 74 ± 2° for PLA-OH. Degradation of ester bonds in PLA in an alkaline medium yields functional groups such as carboxyl and hydroxyl, and these polar groups likely improved the wettability.

The surface morphology of the PLA and PLA-OH scaffolds was characterized by SEM (Fig. 2A) and AFM (Fig. 2B). PLA scaffolds showed the smooth surface morphology whereas the nanoscale rough surface morphology was observed for PLA-OH scaffolds. The roughness (Rq) of the PLA and PLA-OH scaffold surfaces is 0.092 μm and 0.251 μm, respectively. The surface treatment generated nanoscale surface roughness due to polymer degradation and associated polymer erosion. The roughness induced by NaOH treatment may also contribute to the hydrophilicity of the scaffolds [33].

3.2. Surface functionalization of 3D printed scaffolds

The PLA-OH scaffolds were surface functionalized with PEI and followed by conjugation of CA. Fig. 3 depicts various steps involved in performing the surface functionalization on the 3D printed PLA-OH scaffolds. Fig. 3A shows the covalent functionalization of carboxylic groups of PLA-OH scaffolds with the amine groups of PEI moieties using carbodiimide chemistry by forming the amide bond yielding PLA-PEI. Fig. 3B shows a further modification of PLA-PEI with CA also using carbodiimide chemistry for conjugation of PEI and CA to yield PLA-CA. CA is known to mediate the mineralization of HaP on the biocompatible and biodegradable materials when immersed in SBF [34]. PLA-CA was immersed in SBF to deposit HaP on the surface (Fig. 3C).

3.3. Characterization of surface functionalized 3D printed scaffolds

Fig. 4 compiles spectra obtained from XPS to confirm the surface functionalization of PEI and CA on PLA-OH scaffolds. PLA contains three carbon atoms in different chemical states: C—H, C—O and C—OO. The binding energies and the band intensities vary based on the availability of the C atoms in a given functional state. The surface modification by the conjugation of PEI and CA was confirmed based on the intensities of functional groups for C, N and O atoms in the XPS spectra. The spectra obtained at each stage of functionalization were deconvoluted; the peak positions and their relative abundance are listed in Table S2.

Fig. 4A shows the deconvoluted spectra of C1s/3 and O1s/5 for the PLA-OH scaffolds. C—H, C—O, and C—OO of PLA are observed at 284.4, 286.57 and 288.62 eV, respectively. The O1s/5 spectra show two peaks for O—C and O═C at 531.49 and 532.98 eV, respectively. Fig. 4B shows the deconvoluted XPS spectra of PLA-PEI for C1s/3 (284.34, 285.76 and 288.43 eV), O1s/5 (531.80 and 533.31 eV) and N1s/4 (399.57 eV). The same peaks for the PLA were observed but intensities differ. The C—O and C—OO peaks for PLA-PEI show decreased intensity. The spectra for oxygen O1s/5 showed decreased intensity for the O—C peak. The N1s/4 showed that the peak for NH_2 and also for O═CNH where the latter may be ascribed to the nitrogen of the amine functional groups of PEI chains. There is no significant shift between the binding energies for carbon and oxygen peaks in PLA and PLA-PEI.

Fig. 4C shows the deconvoluted spectra for PLA-CA for C1s/3 at 284.53, 286.51 and 288.84 eV, O1s/5 at 531.8 and 533.55 eV and N1s/4 at 399.63 eV. The change in intensities of C, N and O peaks may be attributed to the decreased availability of the functional groups as they were utilized in functionalization steps with PEI and CA. The reduction in the O—C peak and the same in C—O and C—OO peaks indicates

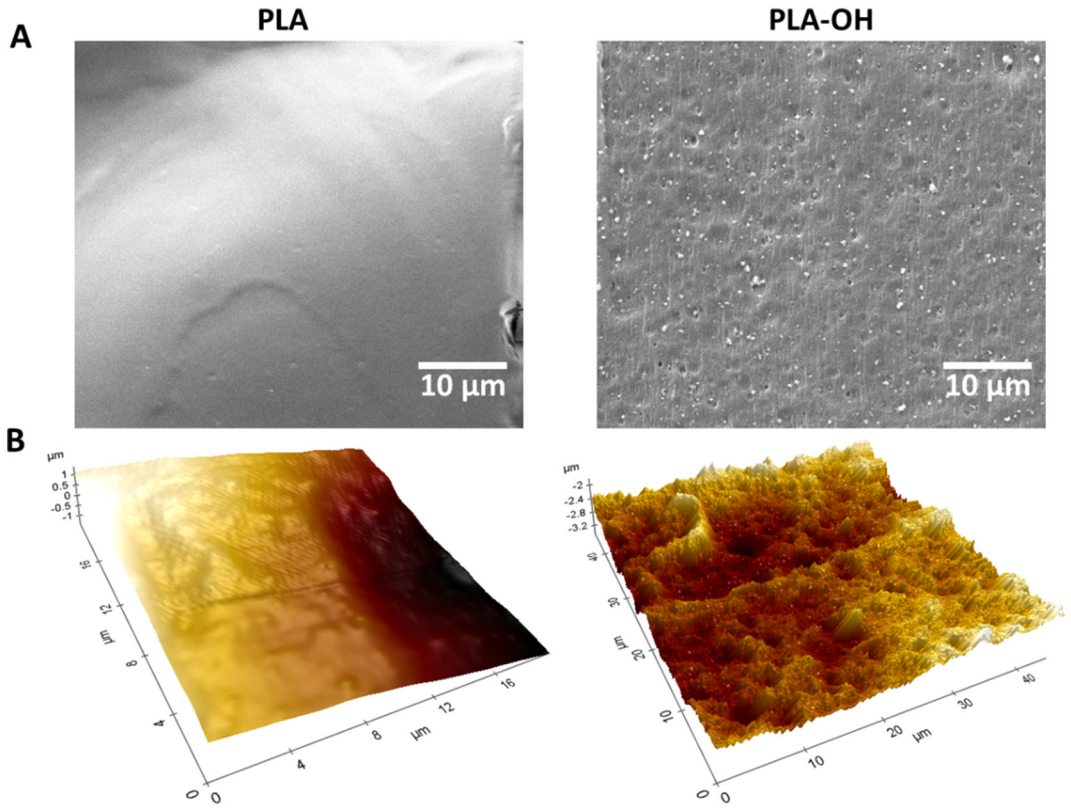

Fig. 2. Characterization of surface treated 3D printed scaffolds [A] SEM images showing the surface morphology of PLA and PLA-OH scaffolds; [B] AFM images showing the 3D view of the nanoscale surface roughness of the PLA and PLA-OH scaffolds.

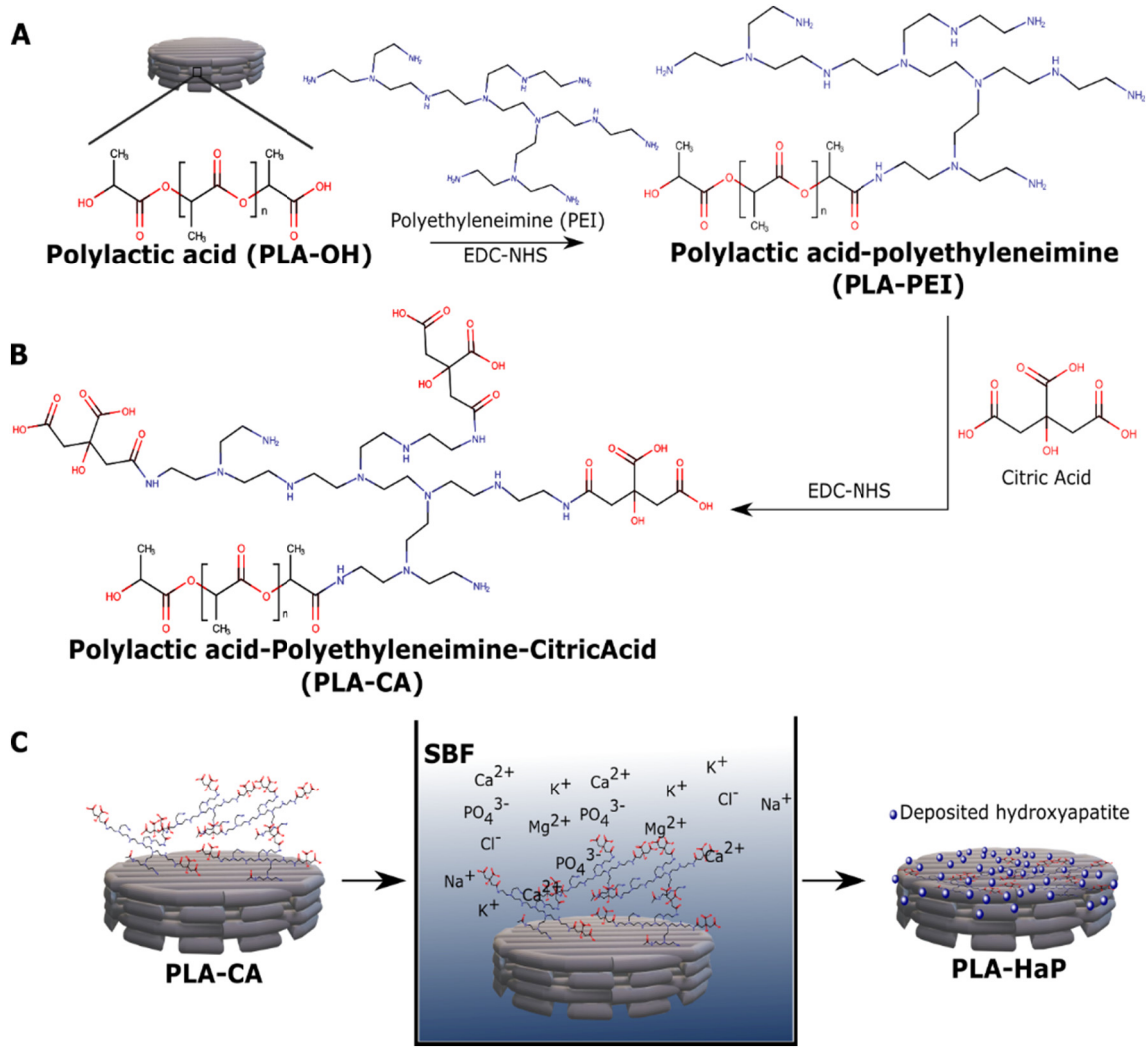

Fig. 3. The schematic showing the steps involved in the functionalization of PLA-OH scaffolds: [A] conjugation of polyethyleneimine by carbodiimide linkage; [B] conjugation of citric acid by carbodiimide linkage; [C] SBF assisted biomimetic deposition of hydroxyapatite on PLA-CA mediated by citric acid yielding PLA-HaP.

that these groups were utilized in forming the peptide bonds with PEI where the N1s/4 peak was observed along with the presence of O═CNH. The further decrease in the intensities in PLA-CA in C, N and O peaks indicate the conjugation of CA to PLA-PEI. This confirms the successful functionalization of PLA-OH with PEI and subsequently CA to the PLA-PEI scaffolds, as shown schematically in Fig. 3.

The surface morphology studied using SEM micrographs of the PLA-OH and other surface modified 3D printed scaffolds at different magnifications are compiled in Fig. 5A–P. At low magnification (Fig. 5A–D), the well aligned layers of the scaffolds can be seen, which were unaltered during surface modification. The magnified images (Fig. 5E–H) show the pore architecture and morphology. The line width and the pore diameter calculated from the SEM images (using ImageJ 1.50i) of the PLA-OH 3D printed scaffolds were found to be 573 ± 22 μm and 314 ± 58 μm, respectively. The marginal increase in strut size and reduction in pore diameter that was noted arise due to the swelling and spreading of the polymer after extrusion through extruder nozzle, which is a common phenomenon of thermal polymer extrusion. Similar observations were reported in the CaP-functionalized PCL scaffolds for bone regeneration [13]. The cross-section micrographs (Fig. 5I–L) reveal the road width (Rw) of 496 ± 52 μm for all the four layers. The orthogonal layer configuration with 0/90° orientation of the polymer struts was observed from the cross-section images. Note that the micrographs indicate that the pores are interconnected. Pore interconnectivity is an essential feature for tissue regeneration in the porous scaffolds. Pore interconnectivity facilitates perfusion of nutrients and augments cell migration deeper into the scaffold. Kumar et al. demonstrated that the open porous structure of 3D printed scaffolds was better than other polymer scaffolds such as foams and fibers in facilitating uniform cell growth through the thickness of the scaffold [35]. In the cross-section images of Fig. 5I–L, the stepwise layout of the Rw is due to the default printer settings as calculated by the Cura software during printing with a line thickness of 150 μm. Hence, for a strut of 500 μm height, the printer has deposited four layers. High magnification SEM images (Fig. 5M–P) revealed that the surface of the scaffold was rough likely due to the NaOH treatment. There were no discernible differences in the surface morphology between PLA-OH (Fig. 5A, E, I, M), PLA-PEI (Fig. 5B, F, J, N), and PLA-CA (Fig. 5C, G, K, O). However, the PLA-HaP scaffolds (Fig. 5D, H, L, P) exhibited bright near-spherical structures, which may be attributed to the formation of apatite on the surface of the scaffolds as a result of the incubation in SBF. EDAX analysis revealed that the calcium to phosphate ratio (Ca/P) of the precipitated minerals on PLA-HaP is 1.57 (Fig. 5Q). This Ca/P ratio is in the range of 1.50 to 1.67 of calcium-deficient HaP (CDHA) [36]. CDHA is one of the many different forms of HaP. The apatite deposition observed on PLA-HaP was also confirmed using XRD (Fig. S2) and several peaks were found to

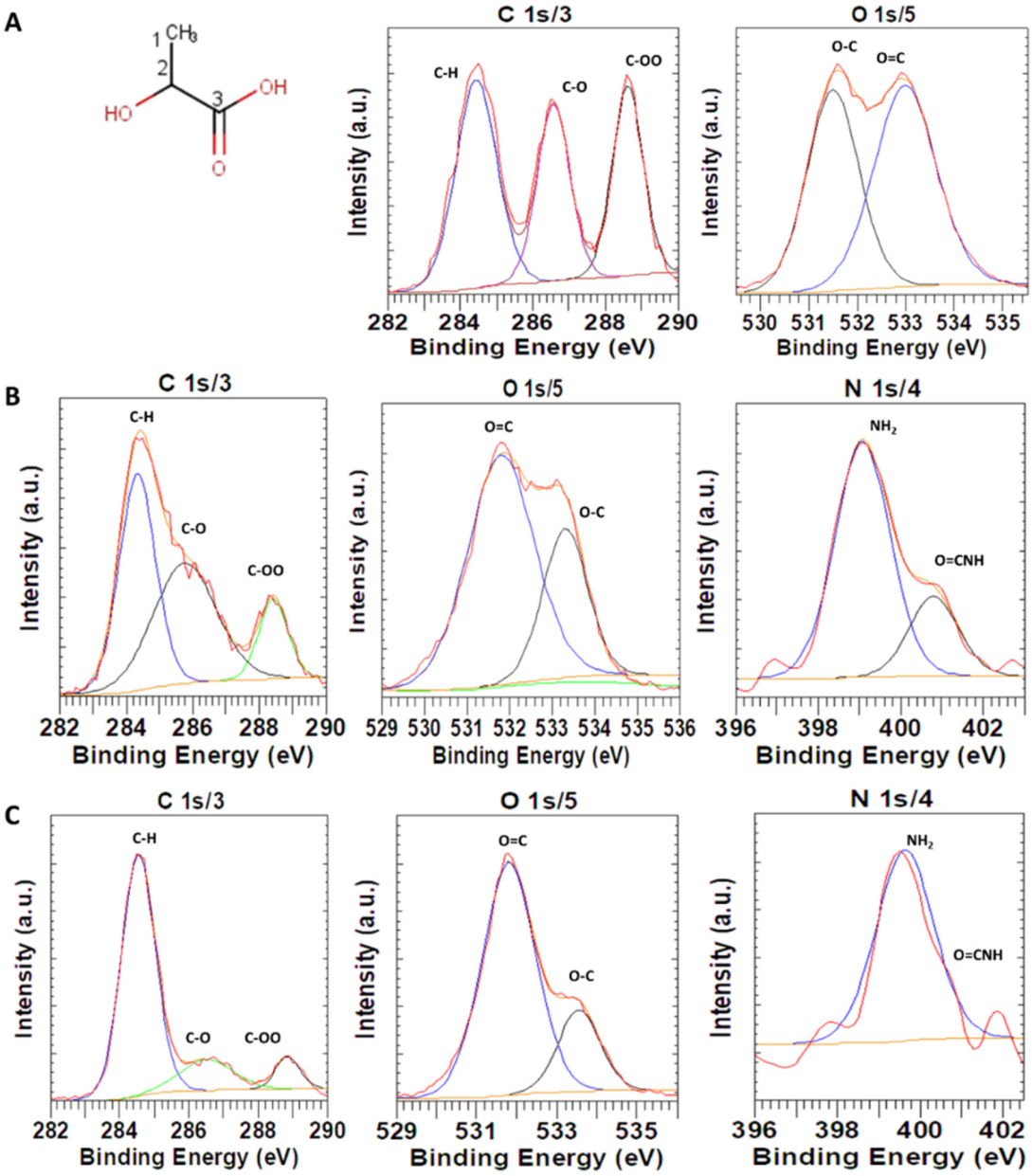

Fig. 4. XPS spectra of surface modified 3D printed scaffolds for the elements C, O and N for [A] PLA-OH, [B] PLA-PEI and [C] PLA-CA.

closely match with the reported pattern for HaP. These results suggest that the surface functionalization of PLA scaffolds has resulted in the successful deposition of HaP on the surface of 3D printed scaffolds.

The water contact angle of the surface functionalized 3D printed scaffolds is compiled in Fig. 5R. NaOH treatment enhanced water wettability of the PLA scaffolds from 124 ± 5° to 74 ± 2°. The PEI modification of PLA-OH marginally increased the contact angle to 78 ± 0.9°, which may be attributed to the aliphatic chains of the branched PEI. The contact angle for PLA-CA was 67 ± 1°, which was reduced due to the surface —COOH groups. As the —COOH groups were covered by mineral deposits in PLA-HaP scaffolds, the contact angle increased to 78 ± 2°. The enhanced surface roughness might have also contributed to the increased water contact angle compared to PLA-CA. Taken together, the surface functionalization strategy herein resulted in a marked increase in the surface wettability compared to the PLA scaffolds.

The 3D printed scaffolds were fabricated with the orthogonal layer configuration of 0/90° orientation because this configuration offers better mechanical properties compared to other displaced layer architecture [24]. Compression tests revealed that the compressive modulus for PLA and PLA-OH scaffolds was 27.5 ± 1.8 and 27.8 ± 0.7 MPa, respectively (Fig. 5S). The surface treatment with NaOH did not affect the mechanical properties. These results are similar to other studies where the compression modulus of PLA 3D printed scaffolds was 25.8 ± 2.7 MPa [25]. The surface modified PLA-PEI (27.1 ± 1.3 MPa) and PLA-CA (26.9 ± 0.5 MPa) scaffolds were also essentially unaffected by the surface treatment. The PLA-HaP scaffolds showed a small but significant increase in the compressive modulus to 29.7 ± 0.5 MPa, compared to all the other scaffolds. Note that the compression moduli of the scaffolds here are higher than the trabecular bone, which is 0.5 to 14.6 MPa [37]. The mineralization on the scaffolds has been reported to have an effect on the mechanical properties due to the presence of the hard-ceramic particles on the PLA-HaP scaffold [25]. TGA analysis revealed that the content of mineral deposits in PLA-HaP was 1.0 wt% (Fig. S3). The PLA-HaP scaffolds incubated in PBS (pH 7.4) exhibited a gradual sustained release of calcium ions from the mineral deposits on the surface of PLA-HaP releasing a cumulative 6% of the total

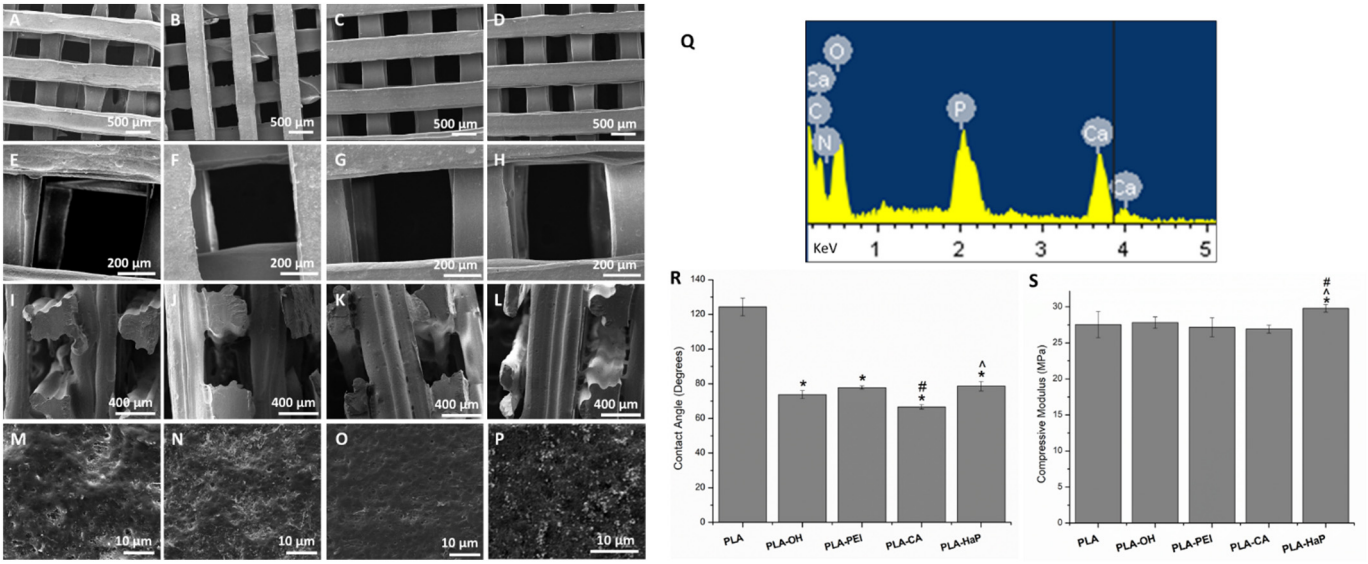

Fig. 5. Characterization of 3D printed PLA and surface modified PLA scaffolds showing [A–P] SEM images of PLA-OH [A, E, I, M]; PLA-PEI [B, F, J, N]; PLA-CA [C, G, K, O] and PLA-HaP [D, H, L, P] at low [A–D] and high [E–H] magnifications, cross section revealing the scaffold features [I–L] and surface features of the functionalized scaffolds [M–P], [Q] EDAX showing Ca and P peaks for elemental analysis of PLA-HaP, [R] Water contact angle measurements of PLA and surface modified scaffolds. Symbols indicate significant difference ($p < 0.05$, one-way ANOVA) between the sample and PLA (*), PLA-PEI (#) and PLA-CA (^), and [S] Compressive modulus of the surface modified scaffolds. Symbols indicate significant difference ($p < 0.05$, one-way ANOVA) between the sample and PLA-OH (*), PLA-PEI (^) and PLA-CA (#). The data are presented as mean ± S.D. for $n = 3$.

deposits in 10 days (Fig. S4). The continuous release of small quantities of calcium ions over prolonged periods was expected to augment stem cell response for bone regeneration [18].

3.4. Cell adhesion and cell proliferation

Toward assessing the bioactivity of the scaffolds for bone tissue regeneration, we studied the response of primary hMSCs in vitro. Bone marrow-derived hMSCs are multipotent stem cells that can potentially differentiate into bone cells, among several other lineages, and hence, play a critical role in bone tissue regeneration in vivo. Cells were cultured on all the different scaffolds and the cell-material interactions were visualized using a combination of SEM and fluorescence microscopy.

Fig. 6A–D shows SEM images of hMSCs cultured on the PLA (Fig. 6A, C) and surface modified PLA-HaP (Fig. 6B, D) scaffolds at day 1 at low (Fig. 6A–B) and high (Fig. 6C–D) magnifications. The yellow color inset shows the typical cell morphology on PLA and PLA-HaP. hMSCs on the PLA-HaP scaffolds showed numerous filopodial protrusions interacting with the mineral deposits on the surface. Note that the cell response observed by SEM was similar on PLA-OH, PLA-PEI, PLA-CA and PLA-HaP. These filopodia signify favorable cell-scaffold interactions and are believed to play an important role in cell migration and matrix remodeling [38]. hMSCs on PLA showed fewer filopodial projections and seem to prefer interactions with the neighboring cells. Studies on cellular interactions with orthopedic biomaterials suggest that rougher surfaces favor cell-material interactions [39]. In addition, the presence of mineral deposits on the PLA-HaP scaffolds provides a biomimetic environment to cells for enhanced cell-material interactions. The PLA-HaP scaffolds are observed to have better cell adhesion than PLA, which could augment cell proliferation and differentiation.

The fluorescence micrographs of hMSCs on PLA, PLA-OH and PLA-HaP scaffolds are compiled in Fig. 6E–J. At day 1 (Fig. 6E–G), the hMSCs on PLA appear thin and slender with minimal spreading. hMSCs on PLA-OH and PLA-HaP exhibit characteristic stem cell morphology and appear well spread on the scaffolds suggesting favorable cell-material interactions. The hMSCs on PLA-PEI and PLA-CA exhibited similar cell morphology (Fig. S5) as observed in PLA-OH and PLA-HaP corroborating the trends observed in SEM. Increased coverage of the scaffolds by day 7 (Fig. 6H–J) suggests cells had proliferated on all the different scaffolds. However, the higher coverage of cells on PLA-OH and PLA-HaP than PLA scaffolds by day 7 suggests that surface treatment enhanced cell attachment and proliferation in agreement with results from SEM images (Fig. 6A–D).

Cell proliferation on the different scaffolds was quantified by WST assay at days 1, 3 and 7 (Fig. 6K). The plot shows a steady increase in cell numbers on all the scaffolds from day 1 to day 3 and day 7 demonstrating that all the scaffolds supported the proliferation of hMSCs. Notably, all the surface modified scaffolds showed a significant increase in cell numbers compared to the untreated PLA on day 1 and day 7 confirming the qualitative observations made in Fig. 6E–J. The surface modified and mineralized PLA-HaP scaffold at day 7 showed the highest cell numbers compared to the other scaffolds and was ~50% higher than the PLA scaffolds. The scaffolds in this study with 70.2% porosity afforded good cell adhesion and proliferation on the surface functionalized scaffolds. Gregor et al. reported good cell proliferation in PLA scaffolds with porosities as low as 30% even though some studies have recommended scaffold porosity of 90% for cell growth [14]. However, high porosity of 90% can severely compromise its mechanical properties for load bearing applications and the scaffold may collapse prematurely as it degrades.

3.5. Osteogenic studies

ALP is an early marker for bone repair and regeneration, which is expressed by the osteoblasts [40]. Fig. 7A presents ALP activity of the differentiating cells on the scaffolds at 14 days. Cells on PLA-HaP showed the highest ALP activity that was significantly higher ($p < 0.05$) than on other scaffolds. ALP activity on PLA-PEI and PLA-CA were marginally higher than on PLA-OH activity although only some of these differences were statistically significant. Hence, the significantly increased expression of ALP by hMSCs cultured on the PLA-HaP scaffolds indicated the enhanced ability of the surface treated scaffolds to facilitate the differentiation of hMSCs to osteoblasts. Note that the PLA scaffold showed poor cell proliferation and thus these as-printed scaffolds were not assessed for ALP activity as the readings were low and the measurements were unreliable.

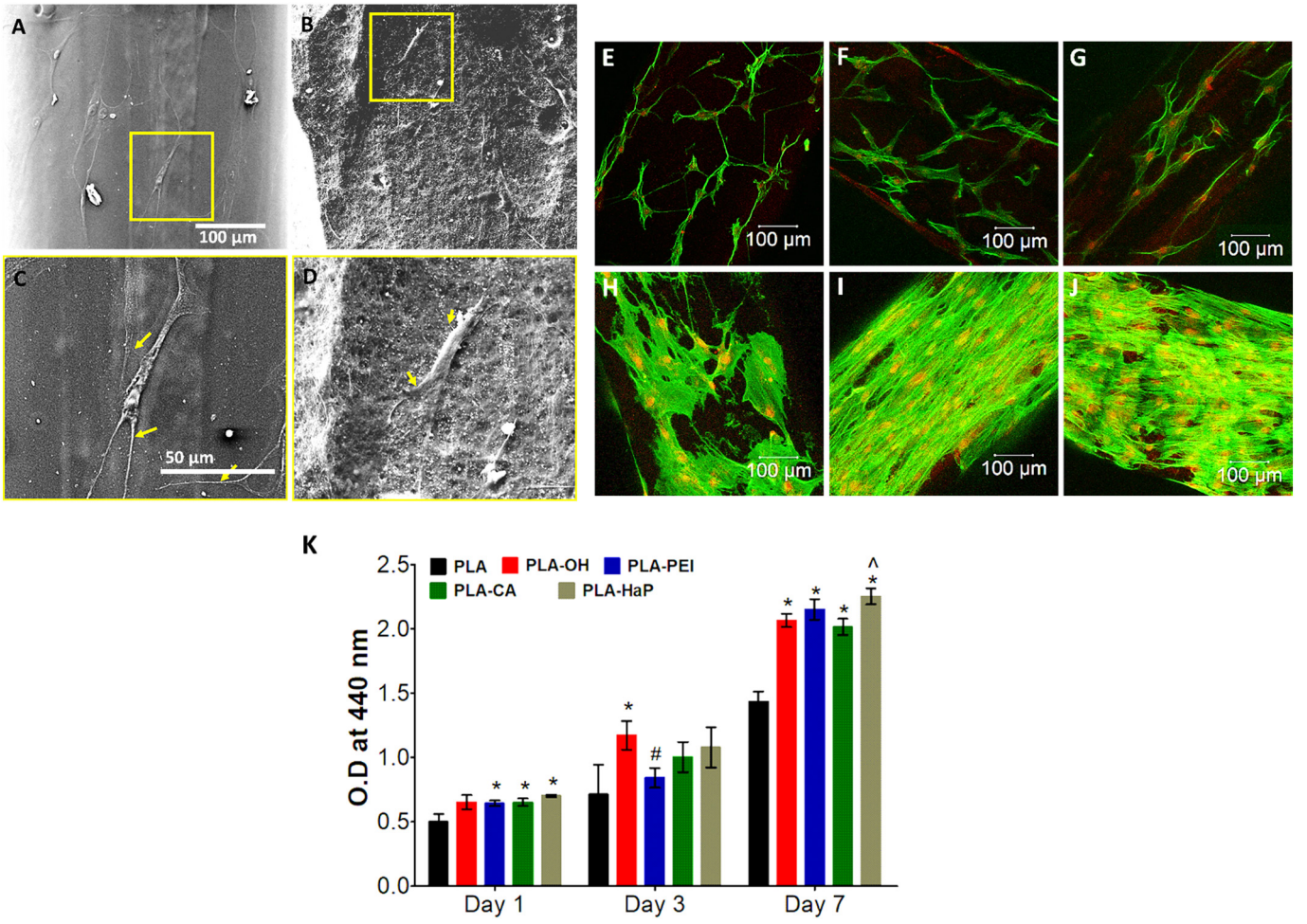

Fig. 6. Response of hMSCs cultured on PLA and surface functionalized 3D printed scaffolds [A–D] The SEM images at low [A–B] and high [C–D] magnifications showing cell attachment at day 1 for PLA [A, C] and PLA-HaP [B, D]; [E–J] Confocal microscopy images of fluorescently labeled cells at day 1 [E–G] and 7 [H–J] showing F-actin (green) and nucleus (red) for PLA [E, H], PLA-OH [F, I], PLA-HaP [G, J] and [K] WST assay showing cell proliferation at days 1, 3 and 7. Symbols indicate significant difference ($p < 0.05$, one-way ANOVA) between the sample and PLA (*), PLA-OH (#) and PLA-CA (^). The data are shown as mean ± S.D. for n = 3.

Alizarin red stains the calcium mineral deposits and was used to visualize deposits resulting from osteogenic differentiation of hMSCs cultured on the scaffolds. Fig. 7B presents photographs of stained scaffolds that can be visualized by the red color. Mineralization on the surface functionalized scaffolds was higher compared to the PLA. PLA-HaP scaffolds showed the highest mineralization. Note that PLA-HaP scaffolds without cells (denoted as PLA-HaP*) showed minimal red color because of the HaP on the surface. The more pronounced red stain on the cell seeded PLA-HaP scaffolds is much higher than that of PLA-HaP* confirming that the mineralization is indeed produced by the differentiated hMSCs. The quantification of mineral deposits by alizarin stain is compiled in Fig. 7C. The PLA-HaP scaffolds showed remarkably higher mineralization than other scaffolds that was 170, 124 and 114% of that on PLA, PLA-OH and PLA-PEI scaffolds, respectively. The presence of HaP as a result of the surface modification of PLA presents a bone-like microenvironment to promote cell differentiation leading to improved mineralization on PLA-HaP scaffolds [7].

3.6. mRNA expression of osteogenic genes

To further confirm the enhanced osteogenic activity of the surface modified PLA-HaP scaffolds, mRNA expression of known osteogenic genes by hMSCs was assessed (Fig. 7D). Note that all data are normalized to PLA-OH as the amount and quality of RNA harvested from PLA scaffolds was inadequate likely due to poor attachment and proliferation of cells. Cells on PLA-HaP scaffolds showed the highest expression of BMP-2, osteocalcin, Runx2, and ALP genes compared to PLA-OH (denoted by the blue horizontal line in Fig. 7D).

BMP-2 is a bone morphogenic protein of the TGFβ family and it is widely accepted as a marker for skeletal development. BMP-2 signaling is known to induce the expression of Runx2, which in turn stimulates the osteogenesis of hMSCs [41]. Cells on PLA-HaP scaffolds showed 2.7-fold higher expression of BMP-2 than on PLA. Runx2 is the early transcriptional factor that is well studied for the bone development and repair. Runx2 also plays an important function in the differentiation of osteoprogenitor cells to osteoblasts facilitating bone mineralization [42]. Runx2 expression by hMSCs on PLA-HaP was 1.1-fold higher. Osteocalcin is an ECM protein, which is also a specific marker for mature osteoblasts [43]. On the PLA-HaP scaffolds, the expression of osteocalcin was 1.13-fold higher. ALP is an enzyme that degrades the inorganic pyrophosphate groups and thus facilitates the mineralization in bone. The cells on PLA-HaP scaffolds showed 1.1-fold higher ALP expression than on PLA-OH scaffolds. The increased expression of the different osteogenic genes indicates that PLA-HaP scaffolds promote osteogenesis of hMSCs that leads to mineralization [44]. Note that changes in gene expression during osteogenesis tend to be small but sufficient to drive phenotypical changes and similar observations were reported earlier [17,45].

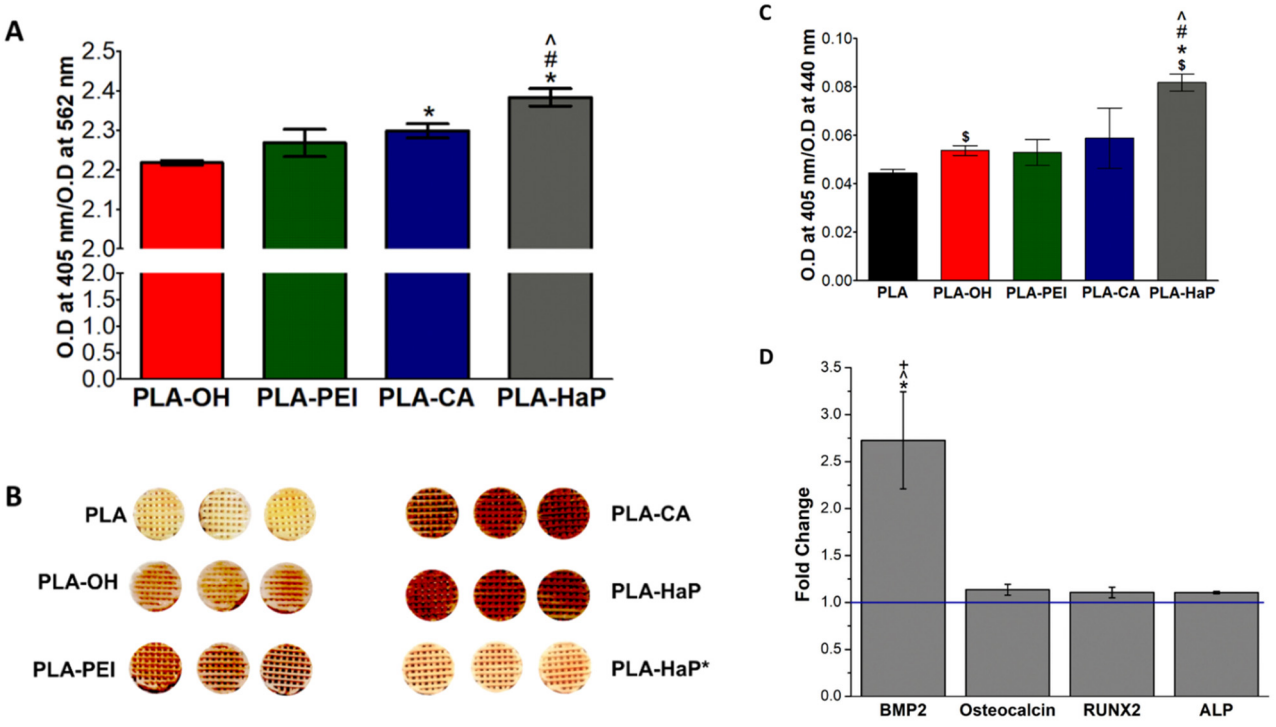

Fig. 7. Osteogenic potential of the 3D scaffolds assessed using hMSCs on the scaffolds for 14 d in the osteogenic medium [A] Quantitative alkaline phosphate activity. Symbols indicate significant difference ($p < 0.05$, one-way ANOVA) between the sample and PLA-OH (*), PLA-PEI (#) and PLA-CA (^), [B] Assessment of mineralization by alizarin red staining of the cell seeded scaffolds. PLA-HaP* denotes as prepared scaffold without cells; [C] Quantification of the stained mineral normalized to cell number. Symbols indicate significant difference ($p < 0.05$, one-way ANOVA) between the sample and PLA ($), PLA-OH (*), PLA-PEI (#) and PLA-CA (^); [D] Quantitative RT-PCR studies of osteogenic markers expressed by hMSCs at day 14 on different scaffolds. The data normalized to the expression of genes on PLA-OH scaffolds as indicated with a blue horizontal line. Symbols indicate significant expression ($p < 0.05$, one-way ANOVA) of BMP2 gene compared to Osteocalcin (*), RUNX2 (^) and ALP (+) genes on PLA-HaP scaffolds. The data are shown as mean ± S.D. for $n = 3$.

4. Discussion

Taken together, the results of this study demonstrate that surface modified PLA-HaP scaffolds are better for bone tissue engineering than neat PLA scaffolds. The enhanced bioactivity observed in this study described above may be attributed to a combination of physical and chemical cues to the stem cells from the surface modified scaffolds. The surface composition of PLA-HaP scaffolds mimics the in vivo microenvironment of the bone cells comprising a composite of polymer and calcium phosphate deposits. The presence of CaP deposits stimulates the stem cells through a variety of routes as follows. Favorable protein adsorption on such a biomimetic surface unlike that on the unmodified polymer surface can augment osteogenesis [46]. Moreover, the HaP deposits on the surface can release calcium ions in the close vicinity of the cells growing on the scaffolds, which are known to promote stem cell osteogenesis [47]. Furthermore, the nanoscale surface roughness due to the HaP deposition also provides topographical cues to promote osteogenic differentiation [48,49]. In fact, it has been shown that the strut surface roughness of 3D printed polymer scaffolds promotes stem cell osteogenic differentiation [50].

In earlier work, the cytocompatibility of PLA 3D printed scaffolds was evaluated by Gregor et al. wherein the scaffolds were found to support proliferation and also the production of osteogenic markers by osteosarcoma cells [14]. Similarly, in the present study, PLA scaffolds (Figs. 5–7) supported cell proliferation and osteogenesis of stem cells. However, the surface modified scaffolds owing to their increased bioactivity by surface functionalization showed enhanced cell proliferation and osteogenic differentiation. HaP and other forms of CaP, which are naturally present in bone tissues can play an important role in imparting bioactivity to the scaffolds for enhanced osteogenesis of stem cells [24]. Ethan et al. reported on the osteogenic differentiation of stem cells on the 3D printed PCL scaffolds functionalized with tricalcium phosphate, HaP and decellularized bone matrix [13]. They demonstrated the increased cell proliferation and osteogenic activity in the ceramic nanocomposite scaffolds. The above strategies involve the formation of composites with polymer and HaP nanoparticles. Although such a strategy can be effective, it requires specialized equipment for the preparation of the polymer/nanoparticle composite filaments prior to 3D printing. Moreover, as discussed above, the concentration of eluted calcium ions is rather limited.

With the rapidly growing popularity of 3D printing to prepare tissue scaffolds, the current work presents a promising strategy to enhance the bioactivity of the scaffolds. Only a few such strategies have been reported recently which utilize introducing nanoscale surface roughness and grafting of peptides on the surface [50,51]. In contrast to these studies, the current strategy is facile, versatile, cost-effective, and can be easily adapted to various biodegradable polyesters, which comprise a significant fraction of 3D printed scaffolds. Expensive biomolecules are not used in this method rendering this a feasible technique for improving the bioactivity of 3D printed bone tissue scaffolds. Moreover, the strategy presented here is remarkably effective with twice the amount of mineral deposited within 14 days on the surface modified scaffolds compared to the PLA scaffolds.

5. Conclusion

Toward developing a surface engineering strategy to promote osteogenesis, 3D printed porous PLA scaffolds were functionalized with PEI and CA, and subsequently modified with CaP mineral deposits. These CDHA deposits presented a bone tissue-like microenvironment to the cells. The PLA-HaP scaffolds showed improved wettability, imparted nanoscale roughness, marginally improved the mechanical properties of the PLAs scaffold and exhibited sustained release of calcium ions in aqueous medium. Consequently, hMSCs showed increased

cell adhesion and cell proliferation as well as marked enhancement of osteogenic differentiation on the surface modified PLA scaffolds compared the as-printed scaffolds. The mineralization on the surface modified scaffolds was twice that on the as-printed scaffolds underscoring the effectiveness of this strategy in contrast to earlier methods. This work presents a potent strategy to modify the surface of 3D printed polymer scaffolds to enhance the osteogenic activity for bone tissue engineering.

CRediT authorship contribution statement

L.R. Jaidev: Conceptualization, Data curation, Formal analysis, Funding acquisition, Investigation, Methodology, Writing - original draft. **Kaushik Chatterjee:** Conceptualization, Formal analysis, Funding acquisition, Methodology, Project administration, Resources, Supervision, Writing - review & editing.

Acknowledgements

The authors thank the Department of Science and Technology, India for funding. The authors are also grateful to Indian Institute of Science and the Department of Materials Engineering for access to instruments. LRJ was supported by Research Associateship from the Council of Scientific and Industrial Research (CSIR), India.

Appendix A. Supplementary data

Supplementary data to this article can be found online at https://doi.org/10.1016/j.matdes.2018.11.018.

References

[1] G. Turnbull, J. Clarke, F. Picard, P. Riches, L. Jia, F. Han, B. Li, W. Shu, 3D bioactive composite scaffolds for bone tissue engineering, Bioactive Mater. 3 (2017) 278–314.
[2] B. Derby, Printing and prototyping of tissues and scaffolds, Science 338 (2012) 921–926.
[3] S.H. Jariwala, G.S. Lewis, Z.J. Bushman, J.H. Adair, H.J. Donahue, 3d printing of personalized artificial bone scaffolds, 3D Print. Addit. Manuf. 2 (2015) 56–64.
[4] H.N. Chia, G. Wu, T.L. Weiss, B.K. Gu, J.D. Wardyn, C.E. Dombroski, 3D Printing in Medicine, Scientific Research Publishing, 2016.
[5] A.V. Do, B. Khorsand, S.M. Geary, A.K. Salem, 3D printing of scaffolds for tissue regeneration applications, Adv. Healthc. Mater. 4 (2015) 1742–1762.
[6] T. Gong, J. Xie, J. Liao, T. Zhang, S. Lin, Y. Lin, Nanomaterials and bone regeneration, Bone Res. 3 (2015), 15029.
[7] J. Ivaska, J. Heino, Adhesion receptors and cell invasion: mechanisms of integrin-guided degradation of extracellular matrix, Cell. Mol. Life Sci. 57 (2000) 16–24.
[8] J. Parthasarathy, B. Starly, S. Raman, A design for the additive manufacture of functionally graded porous structures with tailored mechanical properties for biomedical applications, J. Manuf. Process. 13 (2011) 160–170.
[9] B. Yuan, S.Y. Zhou, X.S. Chen, Rapid prototyping technology and its application in bone tissue engineering, J Zhejiang Univ Sci B 18 (2017) 303–315.
[10] S. Bose, S. Vahabzadeh, A. Bandyopadhyay, Bone tissue engineering using 3D printing, Mater. Today 16 (2013) 496–504.
[11] M.A. Nowicki, N.J. Castro, M.W. Plesniak, L.G. Zhang, 3D printing of novel osteochondral scaffolds with graded microstructure, Nanotechnology 27 (2016), 414001.
[12] C. Zhou, K. Yang, K. Wang, X. Pei, Z. Dong, Y. Hong, X. Zhang, Combination of fused deposition modeling and gas foaming technique to fabricated hierarchical macro/microporous polymer scaffolds, Mater. Des. 109 (2016) 415–424.
[13] E. Nyberg, A. Rindone, A. Dorafshar, W.L. Grayson, Comparison of 3D-printed poly-ε-caprolactone scaffolds functionalized with tricalcium phosphate, hydroxyapatite, bio-oss, or decellularized bone matrix, Tissue Eng. A 23 (2017) 503–514.
[14] A. Gregor, E. Filová, M. Novák, J. Kronek, H. Chlup, M. Buzgo, V. Blahnová, V. Lukášová, M. Bartoš, A. Nečas, Designing of PLA scaffolds for bone tissue replacement fabricated by ordinary commercial 3D printer, J. Biol. Eng. 11 (2017) 31.
[15] I. Zein, D.W. Hutmacher, K.C. Tan, S.H. Teoh, Fused deposition modeling of novel scaffold architectures for tissue engineering applications, Biomaterials 23 (2002) 1169–1185.
[16] J.M. Hong, B.J. Kim, J.-H. Shim, K.S. Kang, K.-J. Kim, J.W. Rhie, H.J. Cha, D.-W. Cho, Enhancement of bone regeneration through facile surface functionalization of solid freeform fabrication-based three-dimensional scaffolds using mussel adhesive proteins, Acta Biomater. 8 (2012) 2578–2586.
[17] M. Chen, D.Q. Le, A. Baatrup, J.V. Nygaard, S. Hein, L. Bjerre, M. Kassem, X. Zou, C. Bünger, Self-assembled composite matrix in a hierarchical 3-D scaffold for bone tissue engineering, Acta Biomater. 7 (2011) 2244–2255.
[18] X. Niu, Z. Liu, F. Tian, S. Chen, L. Lei, T. Jiang, Q. Feng, Y. Fan, Sustained delivery of calcium and orthophosphate ions from amorphous calcium phosphate and poly (L-lactic acid)-based electrospinning nanofibrous scaffold, Sci. Rep. 7 (2017), 45655.
[19] S.R.K. Meka, S. Jain, K. Chatterjee, Strontium eluting nanofibers augment stem cell osteogenesis for bone tissue regeneration, Colloids Surf. B: Biointerfaces 146 (2016) 649–656.
[20] Y. Deng, C. Jiang, C. Li, T. Li, M. Peng, J. Wang, K. Dai, 3D printed scaffolds of calcium silicate-doped β-TCP synergize with co-cultured endothelial and stromal cells to promote vascularization and bone formation, Sci. Rep. 7 (2017) 5588.
[21] S. Kumar, S. Raj, S. Jain, K. Chatterjee, Multifunctional biodegradable polymer nanocomposite incorporating graphene-silver hybrid for biomedical applications, Mater. Des. 108 (2016) 319–332.
[22] L. Jaidev, S. Kumar, K. Chatterjee, Multi-biofunctional polymer graphene composite for bone tissue regeneration that elutes copper ions to impart angiogenic, osteogenic and bactericidal properties, Colloids Surf. B: Biointerfaces 159 (2017) 293–302.
[23] K. Chatterjee, L. Sun, L.C. Chow, M.F. Young, C.G. Simon, Combinatorial screening of osteoblast response to 3D calcium phosphate/poly (ε-caprolactone) scaffolds using gradients and arrays, Biomaterials 32 (2011) 1361–1369.
[24] T. Serra, J.A. Planell, M. Navarro, High-resolution PLA-based composite scaffolds via 3-D printing technology, Acta Biomater. 9 (2013) 5521–5530.
[25] F. Senatov, K. Niaza, M.Y. Zadorozhnyy, A. Maksimkin, S. Kaloshkin, Y. Estrin, Mechanical properties and shape memory effect of 3D-printed PLA-based porous scaffolds, J. Mech. Behav. Biomed. Mater. 57 (2016) 139–148.
[26] T. Kokubo, H. Takadama, How useful is SBF in predicting in vivo bone bioactivity? Biomaterials 27 (2006) 2907–2915.
[27] Y.-Y. Hu, A. Rawal, K. Schmidt-Rohr, Strongly bound citrate stabilizes the apatite nanocrystals in bone, Proc. Natl. Acad. Sci. 107 (2010) 22425–22429.
[28] R.T. Tran, L. Wang, C. Zhang, M. Huang, W. Tang, C. Zhang, Z. Zhang, D. Jin, B. Banik, J.L. Brown, Synthesis and characterization of biomimetic citrate-based biodegradable composites, J. Biomed. Mater. Res. A 102 (2014) 2521–2532.
[29] S.-H. Rhee, J. Tanaka, Effect of citric acid on the nucleation of hydroxyapatite in a simulated body fluid, Biomaterials 20 (1999) 2155–2160.
[30] S. Kumar, S. Raj, K. Sarkar, K. Chatterjee, Engineering a multi-biofunctional composite using poly (ethylenimine) decorated graphene oxide for bone tissue regeneration, Nanoscale 8 (2016) 6820–6836.
[31] K. Sarkar, S.R.K. Meka, G. Madras, K. Chatterjee, A self-assembling polycationic nanocarrier that exhibits exceptional gene transfection efficiency, RSC Adv. 5 (2015) 91619–91632.
[32] G. Caetano, R. Violante, A.B. Sant, A.B. Murashima, M. Domingos, A. Gibson, P. Bártolo, M.A. Frade, Cellularized versus decellularized scaffolds for bone regeneration, Mater. Lett. 182 (2016) 318–322.
[33] M. Wang, P. Favi, X. Cheng, N.H. Golshan, K.S. Ziemer, M. Keidar, T.J. Webster, Cold atmospheric plasma (CAP) surface nanomodified 3D printed polylactic acid (PLA) scaffolds for bone regeneration, Acta Biomater. 46 (2016) 256–265.
[34] J. Chen, B. Chu, B.S. Hsiao, Mineralization of hydroxyapatite in electrospun nanofibrous poly (L-lactic acid) scaffolds, J. Biomed. Mater. Res. A 79 (2006) 307–317.
[35] G. Kumar, C.K. Tison, K. Chatterjee, P.S. Pine, J.H. McDaniel, M.L. Salit, M.F. Young, C.G. Simon, The determination of stem cell fate by 3D scaffold structures through the control of cell shape, Biomaterials 32 (2011) 9188–9196.
[36] M. Bohner, Calcium orthophosphates in medicine: from ceramics to calcium phosphate cements, Injury 31 (2000) D37–D47.
[37] S.A. Goldstein, The mechanical properties of trabecular bone: dependence on anatomic location and function, J. Biomech. 20 (1987) 1055–1061.
[38] G. Mattei, C. Ferretti, A. Tirella, A. Ahluwalia, M. Mattioli-Belmonte, Decoupling the role of stiffness from other hydroxyapatite signalling cues in periosteal derived stem cell differentiation, Sci. Rep. 5 (2015) 10778.
[39] B.L. Banik, T.R. Riley, C.J. Platt, J.L. Brown, Human mesenchymal stem cell morphology and migration on microtextured titanium, Front. Bioeng. Biotechnol. 4 (2016) 41.
[40] L. Kuru, G.S. Griffiths, A. Petrie, I. Olsen, Alkaline phosphatase activity is up regulated in regenerating human periodontal cells, J. Periodontal Res. 34 (1999) 123–127.
[41] A. Javed, J.-S. Bae, F. Afzal, S. Gutierrez, J. Pratap, S.K. Zaidi, Y. Lou, A.J. Van Wijnen, J.L. Stein, G.S. Stein, Structural coupling of Smad and Runx2 for execution of the BMP2 osteogenic signal, J. Biol. Chem. 283 (2008) 8412–8422.
[42] C. Ferguson, E. Alpern, T. Miclau, J.A. Helms, Does adult fracture repair recapitulate embryonic skeletal formation? Mech. Dev. 87 (1999) 57–66.
[43] S. Tanaka, K. Matsuzaka, D. Sato, T. Inoue, Characteristics of newly formed bone during guided bone regeneration: analysis of cbfa-1, osteocalcin, and VEGF expression, J. Oral Implantol. 33 (2007) 321–326.
[44] T. Osathanon, C.M. Giachelli, M.J. Somerman, Immobilization of alkaline phosphatase on microporous nanofibrous fibrin scaffolds for bone tissue engineering, Biomaterials 30 (2009) 4513–4521.
[45] M.T. Tsai, W.J. Li, R.S. Tuan, W.H. Chang, Modulation of osteogenesis in human mesenchymal stem cells by specific pulsed electromagnetic field stimulation, J. Orthop. Res. 27 (2009) 1169–1174.
[46] K.L. Kilpadi, P.L. Chang, S.L. Bellis, Hydroxylapatite binds more serum proteins, purified integrins, and osteoblast precursor cells than titanium or steel, J. Biomed. Mater. Res. A 57 (2001) 258–267.
[47] F. Viti, M. Landini, A. Mezzelani, L. Petecchia, L. Milanesi, S. Scaglione, Osteogenic differentiation of MSC through calcium signaling activation: transcriptomics and functional analysis, PLoS One 11 (2016), e0148173.

[48] M.J. Dalby, N. Gadegaard, R.O. Oreffo, Harnessing nanotopography and integrin-matrix interactions to influence stem cell fate, Nat. Mater. 13 (2014) 558.
[49] L. Krishna, K. Dhamodaran, C. Jayadev, K. Chatterjee, R. Shetty, S. Khora, D. Das, Nanostructured scaffold as a determinant of stem cell fate, Stem Cell Res Ther 7 (2016) 188.
[50] G. Kumar, M.S. Waters, T.M. Farooque, M.F. Young, C.G. Simon, Freeform fabricated scaffolds with roughened struts that enhance both stem cell proliferation and differentiation by controlling cell shape, Biomaterials 33 (2012) 4022–4030.
[51] S. Li, Y. Xu, J. Yu, M.L. Becker, Enhanced osteogenic activity of poly (ester urea) scaffolds using facile post-3D printing peptide functionalization strategies, Biomaterials 141 (2017) 176–187.